1

2

3

4

5

Improvement of the kinetics of hydrogen release from ammonia

borane confined in silica aerogel

8

9

10

11   Miriam Rueda, Luis Miguel Sanz-Moral, José Juan Segovia, Ángel Martín*

12   Department of Chemical Engineering and Environmental Technology - University of

13   Valladolid

14   TERMOCAL Research Group – University of Valladolid

15

16

17   c/ Doctor Mergelina s/n 47011 Valladolid (Spain)

18   Tel: +34 983423174, e-mail: mamaan@iq.uva.es (Á. Martín)

19

20

1

Improvement of the kinetics of hydrogen release from ammonia borane confined in silica aerogel

Miriam Rueda[1], Luis Miguel Sanz-Moral[1], José Juan Segovia[2], Ángel Martín[1]*

[1]Department of Chemical Engineering and Environmental Technology - University of Valladolid, c/ Doctor Mergelina s/n 47011 Valladolid (Spain)

[2]TERMOCAL Research Group – University of Valladolid, c/ Paseo del Cauce 59 47011 Valladolid (Spain)

Tel: +34 983423174, e-mail: mamaan@iq.uva.es (Á. Martín)

Abstract

Ammonia borane is a promising hydrogen storage material due to its high gravimetric capacity (19.6 % wt), but it also presents limitations such as a slow hydrogen release with a long induction time, a difficult regeneration, or the formation of foams and gaseous by-products during thermolysis. Previous studies have shown that by nanoconfinement of ammonia borane within a porous support some of these limitations can be overcome due to the reduction and stabilization of ammonia borane particle size. However, this effect was only observed with moderate ammonia borane loadings, as with higher loadings the pores of the support became obstructed. In this work, silica aerogels produced by CO_2 drying, with pore volumes up to 2 cm^3/g, have been used to confine ammonia borane. The influence of the amount of ammonia borane loaded on the aerogel support on the thermal and structural properties of the material has been analyzed. It has been found that more than 60 wt% of ammonia borane can be effectively stored in the pores of the aerogel support. The resulting material shows faster hydrogen release kinetics by thermolysis at 80ºC, due to a significant reduction in the mea size of ammonia borane

after confinement and the participation of SiOH and SiOSi groups of silica aerogel in the decomposition mechanism.

1. Introduction

As fossil fuel reserves are increasingly limited and their use constitute a constant source of greenhouse gases and other environmental problems, the development of alternative energy sources is attracting a considerable attention [1, 2]. In contrast with fossil fuels, which can be easily stored and used when needed, the production of energy from most renewable sources is variable and it cannot be directly controlled. A possible solution for this limitation could be to use hydrogen (H_2) as an energy vector, according to the approach commonly known as 'hydrogen economy' or 'hydrogen society' [3]: Hydrogen can be produced from water (by electrolysis, thermal decomposition, thermochemical processes, photolysis etc.) using renewable energy sources, and stored until needed. Furthermore, the efficiency of the combustion of hydrogen (by combustion in internal combustion engines, catalytic combustion or fuel cells) is high, and it is one of the most environmentally favorable fuels, as it produces nearly zero gaseous emissions.

At large scales, hydrogen can be transported through pipelines (gas H_2) or tankers (liquid H_2), and it is a good energy vector with an energy density of 33 kwh/kg, containing three times more energy than any hydrocarbon fuel on a weight basis [4]. However, the storage of hydrogen in small mobile units such as vehicles or small electronic equipment is more challenging.

70 These challenges can be quantified analyzing the targets set by the US Department of

71 Energy for 2020 for automotive hydrogen systems: a hydrogen storage gravimetric

72 capacity of 5.5 wt% and a volumetric capacity of 0.040 kg/L, with a maximum cost of

73 333$/kg H_2 stored [5]. Hydrogen storage by some of most obvious systems using

74 compressed or condensed H_2 cannot fulfill these requirements due to the physical

75 properties of hydrogen. In the former case, high pressures (700 bar to reach a volumetric

76 concentration of 0.042 kg H_2/L) or huge volumes are needed, and in the latter, high

77 energy consumption is unavoidable in order to maintain the required cryogenic

78 temperatures [6]. For these reasons, solid state hydrogen storage materials have been

79 intensively studied, as hydrates [7], metal-organic frameworks [8] or metallic and

80 chemical hydrides [9].

81 Ammonia borane (AB) is considered as a promising chemical hydride, due to its high

82 hydrogen gravimetric capacity (19.6%wt H_2) and volumetric capacity (140 g/L),

83 moderate decomposition temperature, non-toxicity [10] and stability at room

84 temperature, even in the range 50-60ºC, which is important from the point of view of

85 safety and engineering implications [11]. The thermal decomposition of neat AB

86 releases one mole of hydrogen per mole of AB in each of the following reactions (1),

87 (2) and (3) [12]. In the first decomposition step, AB releases H_2 forming a complex

88 polymeric aminoborane (PAB) below its melting point (114 ºC):

89 $\quad\quad\quad BH_3NH_3 \rightarrow BH_2NH_2 + H_2 \quad\quad\quad\quad\quad T > 120ºC \quad\quad (1)$
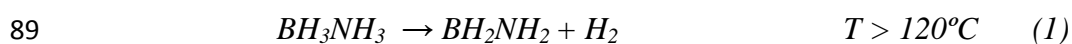
90 Thereafter, PAB decomposes above 120 ºC, forming polymeric iminoborane and small

91 fractions of undesirable volatile byproducts:

92 $\quad\quad\quad\quad BH_2NH_2 \rightarrow 1/3\ (BHNH)_3 + H_2 \quad\quad\quad T > 120ºC \quad (2)$

93 $\quad\quad\quad\quad (BHNH) \rightarrow BN + H_2 \quad\quad\quad\quad\quad\quad T > 500ºC \quad (3)$

94 Nevertheless, the use of this compound as hydrogen storage material also faces some

important limitations. One of them is the kinetic limitation due to the long induction time needed to disrupt the dihydrogen bonding and initiate the release of hydrogen. Furthermore, AB is difficult to regenerate: after thermolysis, it is not possible to restore the initial AB by direct hydrogenation, and complex chemical regeneration routes comprising several steps are needed. Additionally, it forms foams during thermolysis that also complicate the regeneration due to the disruption of the physical structure of the material. Moreover, during the decomposition process, the emission of some volatile byproducts as borazine, diborane or ammonia can be released which could be poisonous for downstream processes and, particularly, hydrogen fuel cells.

Several strategies have been tested to overcome these barriers, including the addition of catalysts as silicon (Si), nickel (Ni), ruthenium (Ru), palladium (Pd) or zinc (Zn) [13-16], confinement of ammonia borane into porous solid supports [17-21], dissolution of AB in ionic liquids [22,23] or using polymers composites [24]. Regarding confinement of AB, different supports have been tested: silica scaffolds as SBA-15 or MCM-48 [18], metal organic frameworks (MOF) [16, 25] or carbon based materials [17] among others. The amount of AB that has been successfully loaded in the support depends on their structural properties (S_{BET} and V_{pores}), getting a maximum amount of 50%wt using silica scaffolds [17]. In all the cases that have been reported, hydrogen kinetic and thermodynamic properties have been improved respect to neat hydride due to the reduction in mean size. In our previous work [26], microparticles of silica aerogel were used as support, getting a maximum concentration of 5%wt AB loaded in hydrophobic silica aerogel. Liquid antisolvent technique was used to precipitate the hydride prior supercritical carbon dioxide drying, resulting in enhanced hydrogen release kinetic compared to pure AB.

In this work, we report the confinement of AB using silica aerogel as porous host. The

120   aerogel has been produced by liquid or supercritical CO_2 drying, a technique that

121   enables to produce a silica material with a high pore volume, and a correspondingly

122   high potential capacity for storage of ammonia borane inside its pores. Several samples

123   with different concentrations of AB up to 60 wt% have been prepared in order to

124   analyze the influence of the loading of AB on the thermal and structural properties of

125   the material. Scanning electron microscopy, N_2 adsorption isotherms, FT-IR

126   spectroscopy and X-ray diffraction have been used in order to characterize the final

127   product prior to the measurement of hydrogen release kinetics by decomposition at

128   80ºC.

129

130   **2. Experimental methods**

131   <u>2.1 Materials</u>

132   Tetramethylorthosilicate (TMOS, 98.0% purity), ammonium hydroxide (NH_4OH, 28.0-

133   30.0% ammonia purity) and ammonia borane (AB, 97% purity) were supplied by

134   Sigma-Aldrich. Figure 1 shows a micrograph of neat AB as received. As shown in this

135   Figure, AB was constituted by agglomerated particles with sizes in the range of 100 μm

136   and with a porous structure. Methanol (MeOH; 99.8% purity), n-hexane (95% purity)

137   and dry tetrahydrofuran (THF; with maximum water of 0.0075wt %) were purchased

138   from Panreac. Carbon dioxide (CO_2, 99.95% purity) was supplied by Carburos

139   Metálicos S.A.

140   (FIGURE 1)

141   <u>2.2 Preparation of AB loaded in silica aerogel microparticles</u>

142   As presented in Figure 2, the procedure for the preparation of AB-loaded silica aerogel

143   microparticles consists of three key steps: preparation of silica gel microparticles,

6

144   addition of ammonia borane by a wet impregnation method, and drying of the AB-

145   loaded gel particles with pressurized carbon dioxide in order to produce the final, dry

146   AB-loaded aerogel microparticles.

147   (FIGURE 2)

148   In the first step of this procedure, hydrophilic silica alcogel was prepared using the well-

149   known method of hydrolysis condensation sol-gel reaction, using TMOS as precursor

150   and methanol as solvent. While with this procedure it is common to prepare large gel

151   monoliths, in this work the gel was synthetized as microparticles, in order to reduce the

152   possible heat and mass transfer resistances that could be caused by larger aerogel

153   monoliths. To do this, and according to the procedure described in a previous work [26],

154   the sol-gel reaction media was dispersed in hexane under mechanical stirring, in order to

155   obtain small droplets of TMOS in methanol dispersed within the hexane continuous

156   phase. After 10 minutes of mechanical stirring of this mixture with a two bladed axial

157   stirrer set at 600 rpm, an aqueous solution of NH_4OH was added as condensation

158   catalyst, which induced the gelation of TMOS. The molar ratio used was the following:

159   1 mol TMOS: 4.4 mol MeOH: 3.3 mol H_2O: 4.5 mol hexane: 0.08 mol NH_4OH. As

160   methanol or water produced during the condensation reaction can induce the

161   decomposition of ammonia borane during the subsequent drying processes [26], after 2

162   hours of gelation the alcogel microparticles were retrieved and immersed in THF. Gel

163   particles were then kept during 7 days immersed in THF in a closed vessel, to let the gel

164   age and strengthen its structure. During this ageing period, the THF solvent was

165   renewed at least twice in order to remove the last traces of methanol and water.

166   After the ageing process, microparticles of alcogel are ready for wet impregnation,

167   adding a solution of ammonia borane dissolved in THF. This method has the advantage

168   that impregnation can be performed under milder temperature conditions compared to

7

169   melt infiltration, and only one impregnation step is necessary in contrast to incipient

170   impregnation methods [27]. Again, THF was used instead of methanol as solvent in

171   order to avoid methanolysis and therefore the decomposition process of the hydride not

172   only during wet impregnation (due to SiOH groups) but also during drying process [26].

173   Different samples with different concentrations of ammonia borane were prepared,

174   adding different amounts of hydride (0-0.4g AB dissolved in 5mL of THF) to 2 g of

175   microparticles of alcogel (gel before drying, therefore with the pores filled with the

176   organic solvent) in order to study his influence on the properties of the final solid

177   product. With this, concentrations of AB in the final product ranging from 10 to 60 wt%

178   AB were obtained, where the concentration of AB is defined as presented in equation

179   (4):

180    $$\%AB = \frac{gAB}{gAB + gaerogel} \qquad (4)$$

181   The third and last step is the removal of the organic solvent in order to obtain the final,

182   dry AB/SiO_2 particles. The drying method employed is a key aspect that determines the

183   textural properties of the porous support. If the solvent is removed by evaporation or

184   lyophilization, the capillary stresses associated to the formation of vapor-liquid

185   interfaces inside the pores of the support cause fractures and a partial collapse of the

186   pore structure of the material. In the case of SiO_2 matrixes, the materials obtained by

187   these drying methods usually show pore volumes below $0.5 - 1.0$ cm^3/g. Some

188   examples are the well-known SBA-15 or MCM-41 mesoporous silica matrixes. In

189   contrast, if pressurized or supercritical carbon dioxide is used to extract the solvent, the

190   collapse of the pore structure is minimized, because under these conditions carbon

191   dioxide can be completely miscible with the organic solvent, and therefore the

192   extraction proceeds without formation of gas-liquid interfaces and without capillary

stresses. Due to this enhanced preservation of the pore structure, with this method it is possible to reach pore volumes in the range $2 - 4$ cm^3/g [28]. Additionally, during this drying process CO_2 can act as antisolvent for solutes dissolved in the organic solvent, as it is completely miscible with the organic solvent, but it cannot dissolve high-molecular weight solutes dissolved in the organic solvent. This precipitation method is commonly referred in the literature as "Gas Anti Solvent" (GAS) or "Supercritical Anti Solvent" (SAS) precipitation [29,30]. In the case of this work, as ammonia borane is insoluble in CO_2 [26], when the THF-immersed alcogels are mixed with CO_2, AB dissolved in the THF that fills the pores of the alcogels quickly precipitates according to a GAS precipitation mechanism, thus favoring the formation of small particles within the pores of the gels.

In a previous work, it was observed that due the interaction of AB with the SiO_2 matrix, the temperature needed to initiate the decomposition of AB is drastically decreased [26]. Thus, in order to avoid the thermolysis of AB, the drying process was carried out at a near-ambient temperature of 25ºC and at a pressure of 100 bar, thus employing pressurized, liquid CO_2. As in the previous work [26], a batch drying apparatus, depicted in Figure 2, was used. Using this apparatus, the alcogels immersed in THF were loaded into the extraction vessel and the system was pressurized with CO_2 using an air-driven piston pump. The system was slowly pressurized at a rate of 0.5 bar/min in order to avoid breakages in the alcogel/aerogel and mechanical stresses that could damage the structural properties of the final product. Once the desired pressure and temperature were reached, the recirculation pump that connects the extraction vessel with the CO_2 reservoir was connected, thus bubbling CO_2 through the THF-immersed alcogels and enhancing the extraction of the solvent. As CO_2 gradually becomes saturated with the solvent during the extraction process, CO_2 in the system was renewed

218   after a predefined extraction time. In this work, four drying cycles were needed (each

219   cycle lasting 60 min, 60 min, 120 min and finally 40 min) to assure the total elimination

220   of organic solvent from the final solid sample. During the CO_2 renewal step after every

221   cycle, the extraction vessel was isolated closing its inlet-outlet valves and kept at the

222   pressure conditions of the drying process to avoid the damages in the structure of the

223   aerogels that could be caused by repeated pressurization-depressurization processes.

224   The rest of the circuit was depressurized till ambient pressure and refilled with the air-

225   driven pump until the extraction pressure of 100 bar. After the last cycle, the entire

226   system was slowly depressurized at a rate of 0.5 bar/min, and samples were retrieved

227   from the extractor and stored until further analysis.

228   Finally, neat ammonia borane was also recrystallized by GAS process using pressurized

229   CO_2 as antisolvent. These experiments allow evaluating if the recrystallization has a

230   separate, specific influence on the hydrogen release properties of the material. As during

231   aerogel drying AB precipitates inside the pores of the aerogel by a similar mechanism as

232   in these GAS experiments, a similar influence of the recrystallization may be expected

233   that would be combined with the influence of the nanoconfinement within the pores of

234   the aerogel. In these GAS experiments, the same apparatus and experimental procedure

235   previously described for aerogel drying experiments was used, loading the extraction

236   cell with a solution of AB in THF (concentration: 24 mg AB/mL THF).

237   <u>2.3 Characterization of AB loaded in silica aerogel</u>

238   2.3.1 Properties of AB/SiO_2

239   Structural properties were analyzed by Fourier Transform Infrared Spectroscopy (FTIR

240   Bruker, model Alpha with a Platinum-ATR single diffraction sampling module). These

241   analyses were performed before and after dehydrogenation for every concentration of

242   AB loaded in silica aerogel.

243   The N_2 adsorption-desorption isotherms data were acquired using a Micrometrics

244   Analyzer (ASAP 2020) with N_2 at -196ºC as sorbate. Prior to the analyses, the samples

245   loaded with AB were outgassed under vacuum at room temperature for 2 hours and the

246   silica aerogel without any impregnation compound was degassed under vacuum at

247   150ºC for several hours (3-5) until the mass of the sample was constant. Total specific

248   surface areas were determined by the multipoint BET method at $P/P_0 = 0.3$, and total

249   specific pore volumes were evaluated from N_2 uptake at $P/P_0 = 0.99$. Pore sizes were

250   calculated using BJH equations.

251   Scanning electron microscopy (SEM) was performed using a Jeol JSM 820 equipment.

252   Energy Dispersive Microanalysis (EDX) was done with microanalysis Bruker Quantax

253   2000 at 20Kv obtaining 10000 signals/second. No metallic coating pretreatment was

254   necessary prior to analyses.

255   X-ray diffraction (XRD) analyses (model Bruker Discover D8) were done at CuKα

256   radiation, λ=1.5418 Å, 2θ angle ranging from 5º to 7º with a scan rate of 4 s/step and a

257   step size of 0.020º. These analyses were also performed before and after thermal

258   dehydrogenation.

259   2.3.2 Thermal decomposition properties

260   Thermal gravimetric analyses (TGA) were undertaken in a Mettler Toledo TGA system

261   from 30 to 300ºC at 5ºC/min heating rate under a nitrogen flow rate of 60 mL/min.

262   Differential scanning calorimetry (DSC) assays were carried out in a Mettler Toledo

263   model 822e with a ceramic sensor of high sensitivity. Nitrogen gas flow was also used

264   at 60 mL/min, with the same heating rate (5ºC/min) from 0 to 250ºC using 5-8 mg of

265   sample.

266   Kinetic measurements of hydrogen release by thermolysis were carried out using a

267   stainless steel cell of 4.7 mL equipped with a certified pressure transducer model

268   DPI104 provided by GE Druck (Germany), which had an uncertainty of $\pm$ 0.01 bar and

269   was connected to a data acquisition computer. The cell was loaded with about 100 mg

270   of sample, determining the precise sample weight with an analytical balance with an

271   uncertainty of $\pm$ 0.0001 g. Then, the cell was subjected to vacuum, down to an absolute

272   pressure below 0.04 bar. The sample was maintained under vacuum at ambient

273   temperature for at least 30 min, in order to remove small amounts of entrapped gases or

274   moisture that could influence the measurement. Afterwards, the sample was heated to

275   80ºC introducing the cell inside a chromatographic oven. The pressure evolution in the

276   cell was recorded every 10 seconds using the pressure transducer acquisition software.

277   The amount of hydrogen released was calculated from pressure recordings using the

278   Hydrogen Reference Equation of State [31] implemented in the Reference Fluid

279   Thermodynamic and Transport Properties Database (REFPROP) software developed by

280   the National Institute of Standards and Technology (NIST) [32].

281   **3. Results and discussion**

282   3.1 Incorporation of ammonia borane in silica aerogel

283   3.1.1 FT-IR studies of neat AB and AB/SiO$_2$ before thermal decomposition

284   Figure 3 shows the FT-IR spectra of neat and recrystallized AB [33-35], and of samples

285   with AB-loaded silica aerogel with different concentrations of AB. In the spectra of neat

286   AB, absorption peaks from 3000 to 3500 cm^{-1} can be associated to N-H stretching

287   whereas B-H stretching appears in the range 2000-2500cm^{-1}. Other characteristic peaks

288   in the IR of neat AB appear at 1602 cm^{-1} (N-H deformation), 1372 cm^{-1}(which may be

289   attributed to double B-N bonds [33] or N-H bonds [34]), 1155 cm^{-1} (B-H scissor), 1051

290   cm^{-1} (N-B-H rock), and N-B bond in the range 720-800 cm^{-1}. As shown in Figure 3, the

291   FT-IR spectrum of recrystallized AB is nearly identical as that of neat AB, indicating

292   that AB has not undergone degradation during the recrystallization.

293   As presented in Figure 3, the spectrum of silica aerogel shows characteristic peaks at

294   798 cm^{-1} (Si-O-Si bond), 950cm^{-1} (Si-OH) and 436 cm^{-1} (O-Si-O) [36]. Samples with

295   silica aerogel loaded with AB yield a combination of the characteristic spectra of AB

296   and silica. AB peaks corresponding to B- H bonds near 2000-2500cm^{-1} and N-H bonds

297   near 1600 cm^{-1} are particularly prominent. It can be also observed that, as expected,

298   these peaks show higher intensities in samples with higher proportion of AB. These

299   results indicate that AB is present in samples and has also not undergone degradation

300   during drying of silica aerogel with CO_2.

301   (FIGURE 3)

302   3.1.2 Textural properties of AB-loaded silica aerogels

303   Figure 4 shows the nitrogen adsorption and desorption isotherms of different samples,

304   and Table 1 shows the textural properties obtained from these isotherms. All these

305   isotherms correspond to class IV according to the classification of International Union

306   of Pure and Applied Chemistry (IUPAC), which is typical of mesoporous materials.

307   They show hysteresis due to the capillary condensation, which is observed at higher

308   relative pressure in samples with a higher amount of AB.

309   (FIGURE 4)

310   (TABLE 1)

The support obtained in this work shows the typical textural properties of silica aerogels reported in many previous works [37, 38]. Comparing to other mesoporous materials, the surface area of the silica aerogel obtained in this work is similar to that of the Santa Barbara Amorphous (SBA) or MCM silica materials used in previous studies of nanoconfination of AB, but the pore volume is almost twice as high [18, 39], which is a favorable property since this higher pore volume can host a higher concentration of AB.

Moreover, both BET and BJH analyses (see table 1) demonstrate that the surface area and the volume of free pores decrease linearly as concentration of AB increases, variations that correspond well with the amount of AB incorporated into the material [17]. Regarding the BJH distributions of pore volume, the bimodal distribution of the empty support is converted to a unimodal distribution for the sample with highest concentration of AB, as the pores with lower size are filled first with AB, leaving partially empty the biggest ones. In the case of the sample with the highest concentration of AB (60 wt%), only 8% of the pore volume remains free, indicating that this concentration of AB is close to the maximum host capacity of the aerogel. These results suggest that AB was successfully confined inside the pores of the aerogel.

In comparison, in previous works the maximum amount of ammonia borane loaded in SBA or MCM silica supports by a conventional solvent infiltration method was 50 wt% [18, 40], but it was observed that when the concentration of AB was higher than a 33%, it started to aggregate outside the pores of the silica support as the internal pore volume of the material became saturated [25]. In the case of metal organic frameworks (MOF), from 20% wt AB [16] till 50% wt AB [41] has been encapsulated depending on the impregnation method or the MOF used. Also, carbon cryogels have been used as supports employing a wet impregnation method, but achieving a maximum

335   concentration of only 24%wt AB [17] due to the comparatively lower surface area (300

336   m^2/g) and volume of pores (0.70 g/cm^3) of this support.

337   3.2 Structural characterization of AB-loaded silica aerogels

338   3.2.1 Morphology of neat AB, recrystallized AB and AB loaded in silica aerogel

339   Figure 5-A shows a SEM micrograph of AB recrystallized from THF solutions using

340   pressurized CO_2 as antisolvent. As observed in this figure, the compound is

341   recrystallized as highly agglomerated flat particles. Due to this morphology, it is

342   difficult to obtain precise particle size measurements, but the size estimated by image

343   analysis of SEM micrographs is in the range of 0.5 μm of thickness and 5 μm of length,

344   values that are considerably smaller than the dimensions of neat AB particles as

345   presented in Figure 1. Furthermore, the recrystallized particles do not show the porous,

346   intertwined structure observed in neat AB (Figure 1).

347   Figure 5-B shows a micrograph of silica aerogel loaded with a 30 wt% of AB. It can be

348   observed that the host silica material is constituted by prismatic particles of 10 – 20 μm,

349   in agreement with the results obtained in a previous work [26]. Furthermore, in SEM

350   micrographs of AB-SiO_2 samples (Figure 5-B), particles with the flat morphology and

351   the dimensions observed in the recrystallized AB (Figure 5-A) are not observed,

352   suggesting that AB did not precipitate as segregated particles outside the aerogel. This

353   impression is confirmed by the results of mapping assays of silica and nitrogen

354   presented in Figure 5. Silica mapping confirms that all the particles that can be observed

355   in the SEM micrograph presented in Figure 5-B indeed correspond to silica aerogel,

356   while nitrogen mapping show that ammonia borane is dispersed within all these

357   particles and is not present as segregated crystals. Therefore it can be concluded that AB

358   is homogenously embedded in the pores of the aerogel. Similar results were obtained in

15

the mapping of samples with higher concentration of AB, up to the maximum

concentration of 60 wt% tested in this work.

(FIGURE 5)

3.2.2 XRD patterns

Figure 6 shows the XRD pattern of neat ammonia borane, which matches well with

JCPDS reference 01-074-0894 suggesting the typical polycrystalline structure with

tetragonal lattice symmetry, in agreement with literature information about the structure

of AB at ambient temperature [42]. The crystallite size estimated using the Scherrer's

equation formula is 40 nm, and the dominant sharp peak of the pattern is located at

23.75º, corresponding to (110) planes. After recrystallization by GAS process, slight

modifications in the XRD pattern can be observed at $2\theta = 17$ and 30º. A similar

modification can be observed in silica-loaded AB samples, although with less defined

peaks due to the strong signal produced by the silica support. This modification in the

pattern can suggest the formation of diammoniate of diborane (DADB), an isomer of

AB. This compound shows some differences regarding the hydrogen release mechanism

compared to its isomer AB: the temperature for decomposition of DADB is about 10ºC

lower than that of AB, and DADB undergoes solid-phase decomposition without

melting or induction period even at moderate temperature, while AB suffers from a long

induction period prior to H_2 release [43]. Therefore, the formation of this compound

may justify some of the observed thermal properties, as it will be discussed in the

following sections.

Nevertheless, in GAS recrystallized samples, the dominant pattern is equivalent to that

of neat AB, also corresponding to tetragonal crystal structure is observed, although

diffraction peaks are not so well defined, and the estimated crystallite size increases to

383   75 – 150 nm. In the case of AB loaded in silica aerogel, the peaks are merged, therefore

384   suggesting a reduction of crystallinity or an increased inhomogeneity in the properties

385   of the crystals   due to the incorporation in the pores [44]. Additionally, as shown in

386   Figure 5b it can be seen that the XRD pattern of amorphous silica, characterized by a

387   broad peak around 24º, is overlaid to the dominant peaks related to AB. Therefore

388   results show that AB retains its crystalline structure after nanoconfinement within the

389   pores of the aerogel, with estimated crystallite sizes in the range 100 – 200 nm, similar

390   to those obtained by recrystallization of AB by GAS process.

391   (FIGURE 6)

392   3.3 Thermal characterization of AB-loaded silica aerogels

393   Figure 7 shows the differential scanning calorimetry (DSC) traces of neat and

394   recrystallized AB compared to samples in which the hydride is loaded in silica aerogel.

395   In the case of the curve of neat AB, a sharp endothermic peak is observed whose onset

396   temperature (T_{on}=108.5 ºC) and peak temperature (T_p=110.8ºC) is dramatically reduced

397   when AB is loaded in silica aerogel (see table 2). This first peak is associated to the

398   melting point [14] or the dissociation of the intermolecular hydrogen bonding [18]. The

399   reduction or elimination in this first peak suggests that the degree of hydrogen bond in

400   the samples in which AB is embedded in silica aerogel is decreased, favoring the

401   reduction of the induction time. A similar result has been observed when AB was

402   embedded in other silica supports [18]. Regarding recrystallized AB, DSC results also

403   show reduction in the onset and peak endothermic temperatures, maintaining the shape

404   of the curve of neat AB. In this case, variations in characteristic temperatures of the

405   DSC traces can be associated to the reduction in the mean particle size achieved by

406   recrystallization of AB. As described by Varin et al [45], a reduction of particle size

407   into the subicrometric or nanometric scale is generally associated to a reduction of the

17

408   onset and peak temperatures of hydrogen evolution thermal events, due to the

409   destabilization of the material induced by the increased particle surface. Additionally,

410   the reduction of onset temperatures and induction time can be associated to the

411   formation of DADB by recrystallization suggested by XRD assays.

412   Similar results have been obtained in other works where AB is confined in different

413   supports. In the case of SBA and MCM silica supports, reductions in the onset and peak

414   temperatures to 48ºC and 100ºC have been reported [18], but as previously described

415   lower temperatures have been obtained in this work. This fact can be due to the higher

416   volume of pores of aerogel support that avoids the agglomeration of AB in meso-

417   channels. Therefore higher contact between the particle and the surface of the silica

418   aerogel takes place, enhancing the influence of silica surface groups on the

419   decomposition mechanism. In experiments with MOFs [42] or carbon cryogels [17, 20]

420   as supports, similar modifications in the thermal response of the material have been

421   reported. However, Srinivas et al. [16] observed a reduction of 30ºC in the onset and

422   peak temperatures of decomposition using MOFs, whereas in our case a displacement of

423   almost 70ºC is obtained.

424   Moreover, DSC results indicate a reduction of the exothermic enthalpy associated with

425   hydrogen release as the proportion silica/AB is increased. The measured enthalpy of

426   reaction for H_2 release from neat AB is -24.9 kJ/mol AB, which is in good agreement

427   with results reported in literature. However, when the proportion silica/AB is increased,

428   the corresponding enthalpy of reaction changes to -10.9 kJ/mol AB for the sample with

429   60% of AB, and -5.5 kJ/mol AB for the sample with 30% of AB. A reduction of the

430   enthalpy of reaction for H_2 release from AB was also observed by Gutowska et al. [40]

431   in their studies of incorporation of AB in mesoporous SBA-15 silica scaffold. However,

432   these authors report a more drastic variation of the enthalpy to -1.0 kJ/mol AB. These

18

433 authors indicate that the reason for the reduced exothermicity is the suppression of the

434 formation of boron compounds as byproducts of the PAB that is the main

435 decomposition product of AB according to reaction 1, which had the favorable

436 consequence of reducing the production of gaseous byproducts.

437 (TABLE 2)

438 (FIGURE 7)

439 This hypothesis agrees well with the results obtained in this work by TGA assays.

440 Figure 8 shows the results of TGA analysis performed on neat AB and AB-loaded silica

441 aerogel. In the case of neat AB, two important weight loss steps, which correspond to

442 the decomposition of the hydride, are observed: the first one till 129ºC corresponds to a

443 weight loss of 12.7 wt% and the second one, which finishes at 213ºC, corresponds to a

444 weight loss of 27.5 wt%. In comparison, and in agreement with the results of DSC

445 assays, TGA analysis shows that the AB confined in silica aerogel initiates its

446 decomposition at lower temperatures. It is also noticeable that in this case, weight loss

447 is not confined to sharp steps at defined temperatures, but it proceeds continuously over

448 the temperature range studied. In particular, at temperatures above 200ºC, where as

449 previously discussed neat AB does not experience any additional weight losses, a

450 continuous weight loss is still observed in the case of AB confined in aerogel. This

451 result indicates that the third step of the thermal decomposition mechanism, indicated in

452 reaction (3), also begins at lower temperatures in the case of confined AB compared to

453 neat AB. Moreover, as shown in Table 2, in both cases the total weight loss per unit

454 mass of AB in the sample is significantly larger than the maximum amount of hydrogen

455 that can stored in the compound. Similar results have been reported in [18], suggesting

456 that when AB is heated to high temperatures above 200ºC, other gases apart from

457 hydrogen are produced, as borazine, diborane, ammonia, etc. However, analyzing the

19

458   results reported in Table 2, it is noticeable that the total amount of volatile compounds

459   produced by heating up to 300ºC is reduced when AB is confined in silica aerogel. This

460   result, together with the variations in DSC assays of confined AB presented before,

461   suggest that interactions between AB and the silica support are taking place that

462   influence the decomposition mechanism of AB. Such interactions were suggested to

463   happen between AB and hydroxyl groups from the silica surface of the host by Lai et al.

464   [18]. These groups can interact   with the BH_3 group, loosening the covalent bond

465   between BH_3 and NH_3 groups of AB, thus destabilizing and promoting the

466   decomposition of the compound. Furthermore, by this interaction BH_3 is kept bound to

467   the scaffold reducing the production of borazine and precluding the formation of

468   poliiminoborane

469   (FIGURE 8)

470   In figure 9, FTIR of neat AB and AB loaded in silica aerogel is shown before and after

471   dehydrogenation at 80ºC. It is observed that most of the peaks at frequencies related to

472   N-H and B-H bonds are broadened, shifted and decreased of intensity which indicates

473   the disruption of the bonds due to the release of hydrogen [13] in both samples. The

474   same behavior is observed for all the concentrations of AB loaded in silica aerogel,

475   although it is more pronounced at higher concentrations of AB. B-N band in the range

476   700-900 cm^{-1}, which is observed in all the samples, is weakened but is still detected

477   after dehydrogenation; this fact clarifies that B-N is not disrupted and ammonia

478   formation is avoided during the decomposition [14]. On the other hand, in the sample in

479   which AB is loaded, the bonds related to silica are present without any change after

480   thermal treatment due to its stability at these conditions.

481   (FIGURE 9)

20

482 Regarding the crystallinity of the samples after thermal dehydrogenation, figure 10

483 shows XRD analyses of byproduct after isothermal dehydrogenation at 80ºC. According

484 to ICDD 00-019-0418, $2\theta= 20.1º$, $23.6º$ and $41.1º$ are assigned to amorphous PAB

485 $(NH_2BH_2)_5$ [46]. In the case of AB/SiO$_2$ samples, amorphous silica peak is present apart

486 from amorphous PAB byproduct.

487   (FIGURE 10)

488 3.4 Kinetics of hydrogen release by thermolysis at 80ºC

489 Figure 11 shows the kinetics of hydrogen release by thermolysis at 80ºC of neat AB

490 compared with AB confinement in silica aerogel. Results in this figure are normalized

491 reporting the amount of hydrogen released by unit mass of AB in the sample. Due to the

492 design of the cell used to measure kinetics, it was not possible to analyze samples of the

493 gas evolved during themolysis. However, it is assumed that at this temperature, the gas

494 which is released is H_2 [12, 19, 41, 47] and no other volatile gases are present in the gas

495 stream in neat AB nor confined in silica aerogel. Regarding the shape of the curve in

496 neat AB, it follows a sigmoidal kinetic, typical of nucleation and growth pathway, with

497 a long induction time of more than 2 h, as reported in previous works [48]. After

498 confinement in silica, the induction time is reduced significantly. This means that the

499 silica could act as a catalyst (SiOH groups) [40] creating defect sites in the support that

500 initiate the decomposition at lower temperature. On the other hand, at lower

501 concentration of AB in the solution (prior to the drying), the hydride could precipitate in

502 the pores of the silica with lower mean size as was also suggested with XRD analyses

503 and corroborated in BET results. This suggests that smaller particles have more contact

504 with the surface of the silica and an easier way to form different bonds between the two

505 free pair of electrons of O in the Lewis base of Si-O-Si or Si-OH bond from the silica

21

506   with BH_3 or NH_3 from AB. As result, the intermolecular hydrogen bond is reduced,

507   following the mechanism proposed by Lai et al. [18].

508   In the case of neat AB, 2 hours are needed to start releasing H_2, and more than 4 hours

509   to get half of its content in H_2 at this temperature ($0.025gH_2/gAB$) whereas only it takes

510   22 minutes in the case of 13%AB loaded in silica aerogel. This fact shows the

511   improvement of silica aerogel as support for this chemical hydride system.

512   Regarding to recrystallized sample, it can be observed that the release profile maintains

513   the sigmoidal shape characteristic of neat AB, with a slower hydrogen release than

514   samples loaded in silica aerogel during the first 30 min of thermolysis. However,

515   compared with neat AB, with the particle size reduction achieved by GAS

516   recrystallization the induction time is drastically reduced and the release of hydrogen is

517   accelerated, to the point that after one hour an equivalent amount of hydrogen is

518   released from GAS-recrystallized AB as from AB loaded silica aerogel with a 30 wt%

519   of AB.

520   (FIGURE 11)

521   As a complement to Figure 11, Table 3 presents the total hydrogen release per unit mass

522   of solid product (AB + silica aerogel support). Results in this table clearly indicate the

523   weight penalty caused by the use of silica aerogel as porous host, as this material does

524   not contribute to the hydrogen storage capacity, thus reducing the total gravimetric

525   capacity of the material [27]. However, it can be seen that this disadvantage is

526   counterbalanced by a faster hydrogen release during the first 1-2 h of thermolysis.

527   (TABLE 3)

528   Moreover, there is a significant visual change in the morphology of neat AB in contrast

529   to AB encapsulated in silica aerogel. Figure 12 shows the different result of AB after

530 thermal decomposition at 80ºC. In the case of neat AB, foaming process takes place at

531 the same time that H_2 is released from the hydride. Thus, even if the material was

532 micronized before thermolysis, this morphology and its associated advantages are

533 completely lost during the thermolysis and therefore in possible future hydrogen cycles,

534 if the material is regenerated [49]. However, when AB is encapsulated in silica aerogel,

535 this process is avoided obtaining particles with the same physical appearance. To

536 confirm this observation, Figure 13 presents SEM/EDX micrographs of the

537 60%AB/SiO_2 sample after thermolysis. As shown in this figure, the original

538 morphology of the material is preserved after the thermolysis. Furthermore, as indicated

539 by the results of nitrogen mapping, the decomposition products of AB remain

540 homogeneously dispersed within the SiO_2 aerogel matrix. Therefore it can be concluded

541 that by incorporation of AB inside the aerogel the morphological variations of the

542 material due to foaming are avoided.

543 (FIGURE 12)

544 (FIGURE 13)

545 **4. Conclusions**

546 Ammonia Borane has been recrystallized and nanoconfined inside the pores of silica

547 aerogel by a novel process, based on a simultaneous aerogel drying and ammonia

548 borane gas antisolvent precipitation using compressed carbon dioxide. Due to the

549 favorable textural properties of the aerogel materials obtained with this method, it has

550 been possible to load aerogels with up to 60 wt% of ammonia borane, without blocking

551 of pores and with a homogeneous dispersion of ammonia borane within the aerogel. By

552 analysis of the thermolysis process, it has been observed that by nanoconfinement the

553 temperature required to initiate the thermolysis process is reduced and the release

554 kinetics are accelerated as they do not show induction time. Furthermore, by

555 nanoconfinement of AB, the morphological properties of the material are stabilized and

556 foaming is eliminated, which could be favorable properties for a subsequent material

557 regeneration process. The feasibility of implementation of the multi-step chemical

558 process required to re-hydrogenate AB when this compound is embedded in the silica

559 matrix remains to be tested.

560

Supplementary Information

561

562 Video 1: Thermolysis of neat ammonia borane at 80ºC. Time is accelerated by a factor

563 of 64.

564 Video 2: Thermolysis of 60%AB/SiO$_2$ sample at 80ºC. Time is accelerated by a factor

565 of 64.

566

574 **References**

575 [1] M.Balat, Int. J. Hydrogen Energ. 33 (2008) 4013-4029

576 [2] M.Hook, X.Tang, Energ. Policy 52 (2013) 797-809

577 [3] S. A. Sherif, F. Barbir, T. N. Veziroglu, Electricity J. 18 (2005) 62-76

578 [4] J. Graetz, Chem. Soc. Rev. 38 (2009) 73-82

579   [5] DOE: US Department of Energy. Web site: http://www.doe.gov.

580   [6] L. O. Williams, D. E. Spond, Appl. Energ. 6 (1980) 99-112.

581   [7] H. P. Veluswamy, R. Kumar, P. Linga, Appl. Energ.122 (2014) 112-132.

582   [8] M. Paik Suh, H. J. Park, T. K. Prasad, D. Lim, Chem. Rev. 112 (2012) 782-835

583   [9] B.Sakintuna, F.Lamari-Darkrim, M.Hirscher, Int. J. Hydrogen Energ. 32 (2007)

584   1121-1140

585   [10] B. Peng, J. Chen, Energ. Environ. Sci. 1 (2008) 479-483

586   [11] S. D. Rassat, C. L. Aardahl, T. Autrey, R. S. Smith, Energ. Fuel. 24 (2010) 2596-

587   2606

588   [12] G. Wolf, J. Baumann, F. Baitalow, F. P. Hoffmann, Thermochim. Acta 343 (2000)

589   19-25

590   [13] D. Kumar, H. A. Mangalvedekar, S. K. Mahajan, Mater. Renew. Sustain. Energy 3

591   (2014) 23

592   [14] A. C. Gangal, P. Kale, R. Edla, J. Manna, P. Sharma, Int. J. Hydrogen Energ. 37

593   (2012) 6741-6748

594   [15] B. Roy, J. Manna, P. Sharma, J. Alloy Compd. 645 (2015) S234-S238.

595   [16] G. Srinivas, J. Ford, W. Zhou, T. Yildirim, Int. J. Hydrogen Energ. 37 (2012)

596   3633-3638

597   [17] A. Feaver, S. Sepehri, P. Shamberger, A. Stowe, T. Autrey, G. Cao, J. Phys. Chem.

598   B 111, (2007) 7469-7472

599   [18] S-W Lai, H-L. Lin, T.L.Yu, L-P. Lee, B-J. Weng, Int. J. Hydrogen Energ. 37

600   (2012) 14393-14404

601   [19] T.Autrey, A.Gutowska, L.Li, J.Linehan, M.Gutowski, Preprints of Papers-

602   American Chemical Society, Division of Fuel Chemistry 49 (2004) 150-151

603   [20] S.Sepehri, B.B.Garcia, G.Cao, J. Mater. Chem. 18 (2008) 4034-

604   [21] S.Sepehri, A.Feaver, W.J.Shaw, C.J.Howard, Q.Zhang, T.Autrey, G.Cao, J. Phys.

605   Chem. B 111 (2007) 14285-14289

606   [22] R.K.Ahluwalia, J.K.Peng, T.Q.Hua, Int. J. Hydrogen Energ. 36 (2011) 15689-

607   15697

608   [23] M. J. Valero-Pedraza, A. Martín-Cortés, A. Navarrete, M. D. Bermejo, Á. Martín.

609   Kinetics of hydrogen release from dissolutions of ammonia borane in different ionic

610   liquids. Energy 91 (2015) 742-750.

611   [24] S.F.Li, Z.W.Tang, Y.B.Tan, X.B.Yu, J. Phys. Chem. C 116 (2012) 1544-1549

612   [25] L-Q Wang, A.Karkamkar, T.Autrey, G.J.Exarhos, J. Phys. Chem. C 113 (2009)

613   6485-6490

614   [26] M.Rueda, L.M.Sanz-Moral, A. Nieto-Márquez, P.Longone, F.Mattea, A.Martín, J.

615   Supercrit. Fluids 92 (2014) 299-310

616   [27] T. Nielsen, F.Besenbacher, T.R.Jensen, Nanoscale 3, (2011) 2086-2098

617   [28] A.S. Dorcheh, M. H. Abbasi., J. Mater. Process. Tech. 199 (2008) 10-26

618   [29] E. Reverchon, R.Adami, G.Caputo, I. de Marco, J. Supercrit. Fluids 47 (2008) 70-

619   84

620   [30] M.Rueda, L.M Sanz-Moral, A.Martín, Cryst. Growth Des. 14 (2014) 4768-4776

621   [31]J. W. Leachman, R. T. Jacobsen, S. G. Penoncello, E. W. Lemmon, J. Phys. Chem.

622   Ref. Data 38 (2009) 721-748.

623   [32] E. W. Lemmon, M. L. Huber, M. O. McLinden. NIST Standard Reference

624   Database 23: Reference Fluid Thermodynamic and Transport Properties-REFPROP,

625   Version 9.1, National Institute of Standards and Technology, Standard Reference Data

626   Program, Gaithersburg, 2013.

627   [33] M.R.Weismiller, S.Q.Wang, A.Chowdhury, S.T.Thynell, R.A.Yetter, Thermochim.

628   Acta 551 (2013) 110-117

629   [34] F.Leardini, M.J.Valero-Pedraza, E.Perez_Mayoral, R.Centelli, M.A.Bañares, J.

630   Phys. Chem.C 118 (2014) 17221-17230

631   [35] J.Smith, K.S.Seshadri, D.White, J. Mol. Spectrosc. 45, (1973) 327-337

632   [36] R.Al-Oweini, H. El-Rassy, J. Mol. Struct. 919 (2009) 140-145

633   [37] M.Alnaief, I.Smirnova, J. Supercrit. Fluids 55 (2011) 1118-1123

634   [38] S.Smitha, P.Shaiesh, P.R.Aravind, S.R.Kumar, Micropor. Mesopor. Mat. 91 (2006)

635   286-292

636   [39] W-J Son, J-S Choi, W-S Ahn, Micropor. Mesopor. Mat 113 (2008) 31-40

637   [40] A.Gutowska, L.Li, Y.Shin, C.M.Wang, X.S.Li, J.C.Linehan, R.S.Smith, B.D.Kay,

638   B.Schmid, W.Shaw, M.Gutowski, T.Autrey, Angewa. Chem. Int. Ed. 44 (2005) 3578-

639   3582

640   [41] Z.Li, G.Zhu, G.Lu, S.Quiu, X.Yao, J. Am. Chem. Soc. 132 (2010) 1490-1491

641   [42] A.Paolone, O.Palumbo, P.Rispoli, R.Cantelli, T.Autrey, J. Phys. Chem. C 113

642   (2009) 5872-5878

643   [43] Z. Fang, J. Luo, X. Kang, H. Xia, S. Wang, W. Wen., X. Zhou, P. Wang, Phys.

644   Chem. Chem. Phys. 13 (2011) 7508-7513.

645   [44] H.Kim, A.Karkamkar, T.Autrey, P.Chupas, T.Proffen, J. Am. Chem. Soc. 131

646   (2009) 13749-13755

647   [45] R. A. Varin, T. Czujko, Z. S. Wronski. Nanomaterials for Solid State Hydrogen

648   Storage, Springer, New York, 2009.

649   [46] U.B.Demirci, S.Bernard, R:Chiriac, F.Toche, P.Miele, J. Power Sources 196

650   (2011) 279-286

651   [47] F.Baitalow, J.Baumann, G.Wolf, K.Jaenicke-Robler, G.Leitner, Thermochim. Acta

652   391 (2002) 159-168

653 [48] A.C.Stowe, W.J.Shaw, J.C.Linehan, B.Schmid, T.Autrey, Phys. Chem. Chem.

654 Phys. 9 (2007) 1831-1836

655 [49] A.D.Sutton, A.K.Burrel, D.A.Dixon, E.B.Garner, J.C.Gordon, T.Nakagawa,

656 K.C.Ott, J.P.Robinson, M.Vasiliu, Science 331 (2011) 1426-1429

657

681   dehydrogenation at 80ºC. * indicates the peaks related to polyaminoborane (PAB) and +

682   refers to amorphous silica peak

683   **Figure 11. -** Isothermal kinetic of hydrogen releases from AB and AB loaded in silica

684   aerogel with different concentrations at 80ºC. (The curves are normalized according to

685   the amount of AB in the sample)

686   **Figure 12.-** Photographs of neat AB and 60%AB/SiO_2 before and after the isothermal

687   H_2 release by thermolysis at 80ºC a) neat AB before thermolysis, b) neat AB after

688   thermolysis, c) AB/SiO_2 before thermolysis, d) AB-SiO_2 after thermolysis. Video clips

689   of the thermolysis process are provided as Supplementary Information

690   **Figure 13**.- SEM image of 60%AB/SiO_2 sample after thermolysis (A), with results of N

691   (B) and Si (C) mapping.

692

693   **Tables**

694

695   **Table 1.-**BET surface areas and BJH pore volumes and pore diameters of silica aerogel

696   dried with liquid or supercritical CO_2 at and AB-loaded silica aerogel

Sample	BET surface area ($m^2 g^{-1}$)	Pore volume ($cm^3 g^{-1}$)	Pore diameter (nm)
SiO_2 sc drying	723.1±2.0	1.35	7.6
SiO_2 Liquid drying	887.3±1.4	1.94	8.7
13AB/SiO_2	216.6±0.3	0.82	11.1
30AB/SiO_2	137.3±0.3	0.56	10.9
60AB/SiO_2	30.4±0.1	0.17	13.7

697

698

699 **Table 2.** - Temperature data and weight losses of neat and recrystallized AB vs loaded

700 in silica aerogel with different concentration obtained from DSC and TGA analyses

701 respectively.

702

Sample	T_{on1} (ºC)	T_{p1} (ºC)	T_{on2} (ºC)	T_{p2} (ºC)	Total wt loss per wt AB
Neat AB	108.5	110.8	113.9	114.1	40.2
Recrystallized AB	70.5	77.9	102.4	113.4	-
60% AB/SiO$_2$	37.6	62.3	84.8	108.9	33.0
30% AB/SiO$_2$	39.5	68.7	83.1	99.0	-

703 **Table 3. -** Amount of H$_2$ released at different times by isothermal thermolysis at 80ºC in

704 neat and recrystallized vs. AB loaded in silica aerogel with different concentration

Sample	15min mgH$_2$/gtotal	30min mgH$_2$/gtotal	45min mgH$_2$/gtotal	1h mgH$_2$/gtotal	2h mgH$_2$/gtotal	final mgH$_2$/gtotal
neat AB	0	0	0	0	2	52
AB recrystallized	1,66	7,45	20,19	30,45	43,98	52
13%AB/SiO$_2$	2,26	4,28	5,28	5,80	6,38	6,76
30%AB/SiO$_2$	1,69	4,43	7,30	9,07	12,31	14,56
60%AB/SiO$_2$	2,48	9,42	17,79	20,65	27,27	32,24

705

706   **Figures**

707
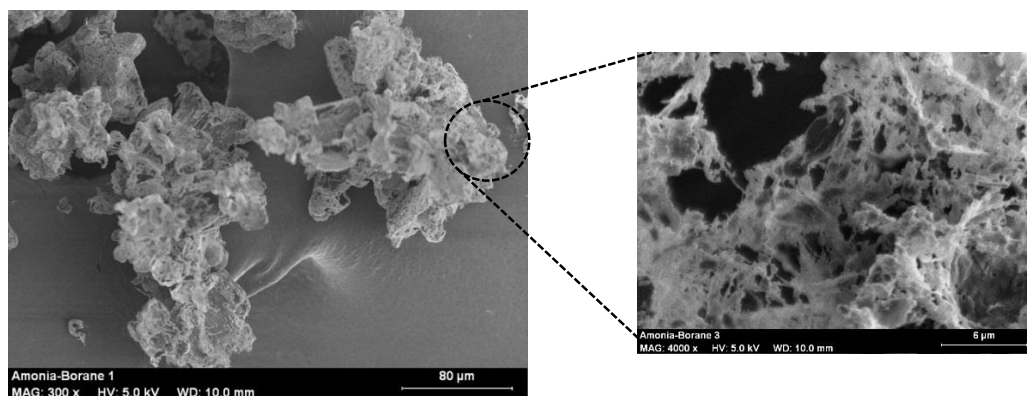
708

709   **Figure 1. -** SEM micrograph of neat ammonia borane as received

710
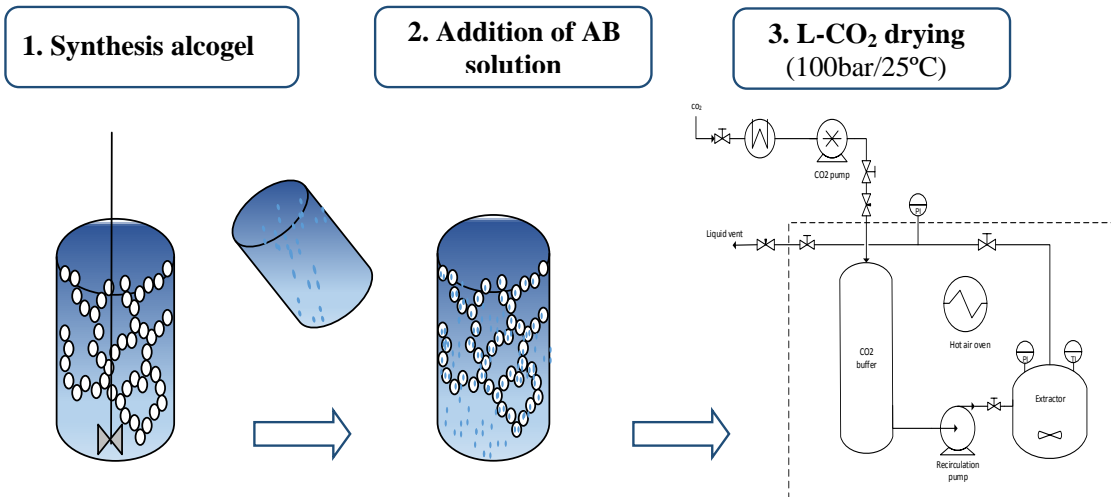
711

712   **Figure 2**. - Steps for preparation of silica aerogel microparticles loaded with ammonia

713   borane.

714
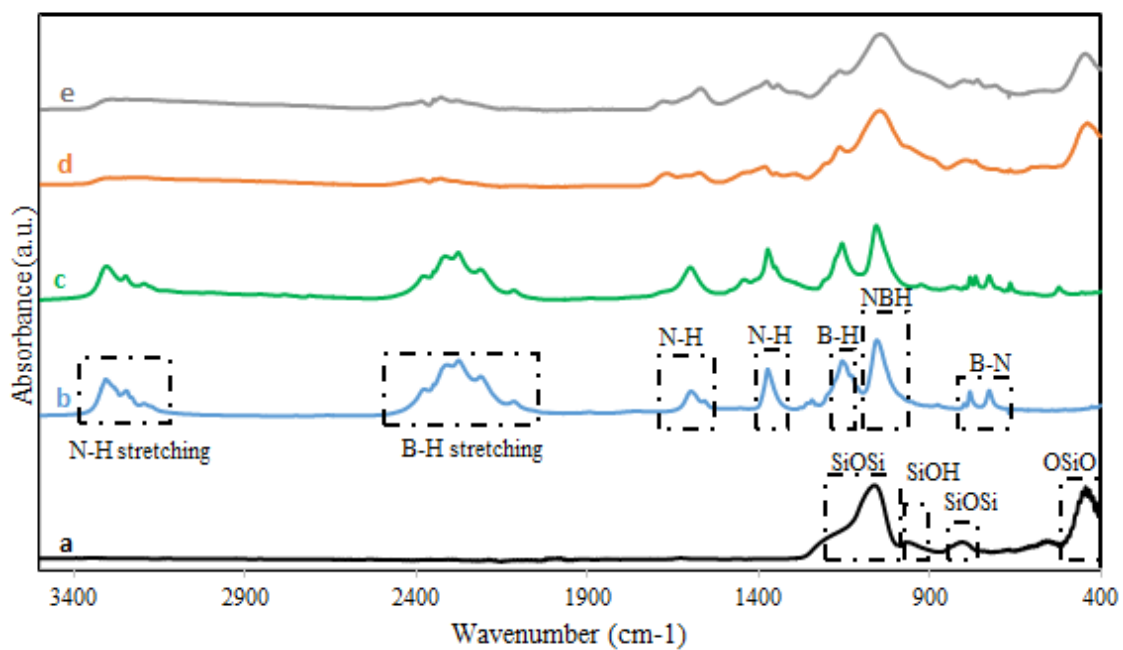
Figure 3. FTIR spectra of a) silica aerogel b) neat AB c) recrystallized AB d)30%AB/SiO$_2$ e)60%AB/SiO$_2$. Curves are vertically displaced for clarity.
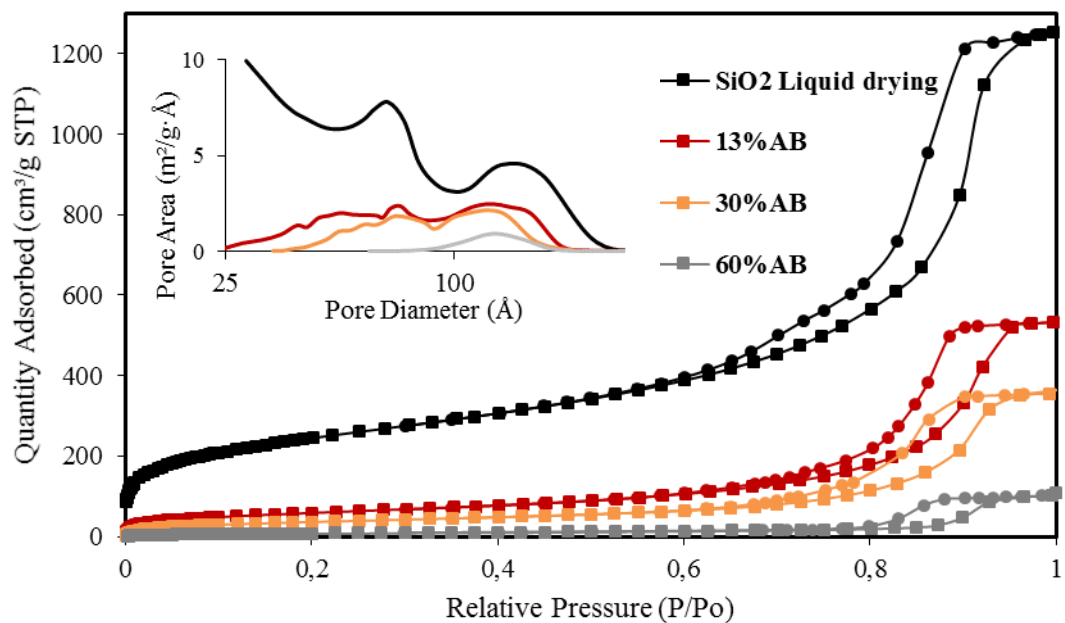
Figure 4.-Nitrogen adsorption-desorption isotherms and BJH pore size distribution of silica aerogel and AB loaded in silica with different concentration (●) adsorption (■) desorption

724
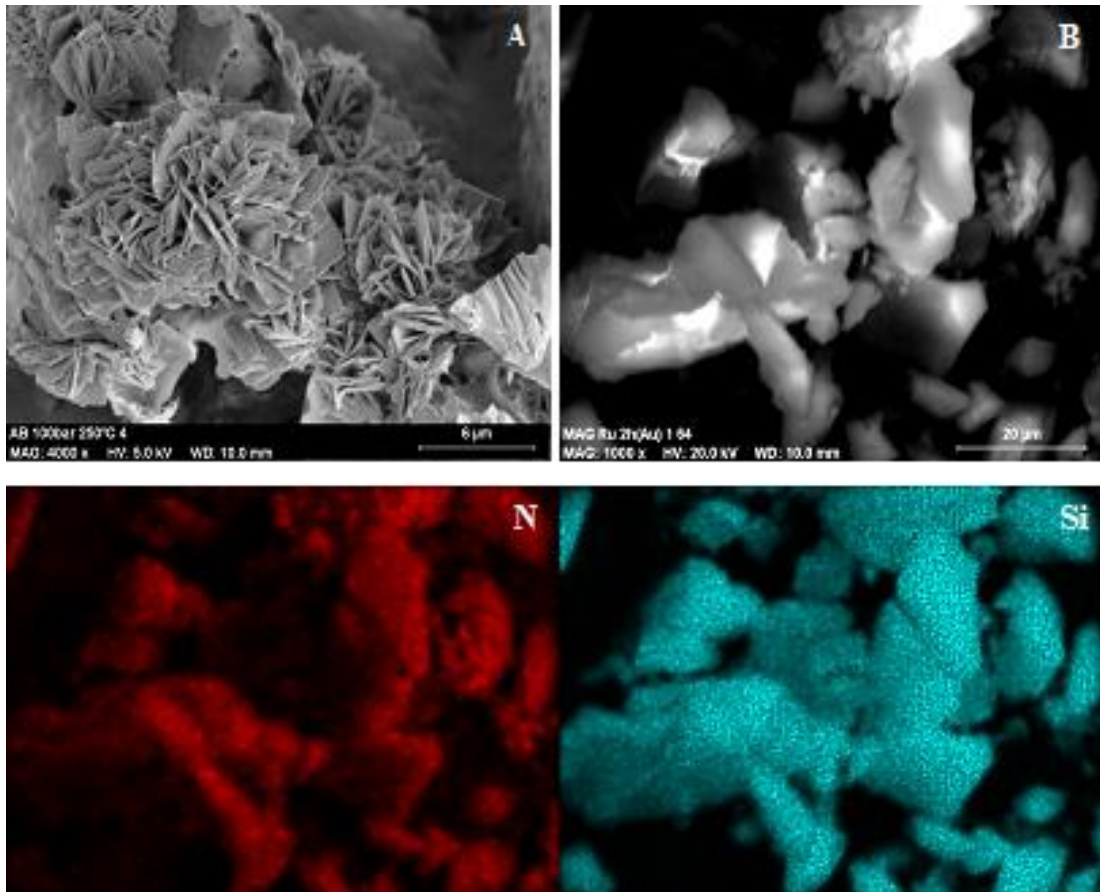
Figure 5.- SEM images of A) Recrystallized AB after recrystallization in THF using

liquid CO_2 as drying method B) 30%AB loaded in silica aerogel and mapping of sample

B (blue is referred to silica and red to Nitrogen)

728
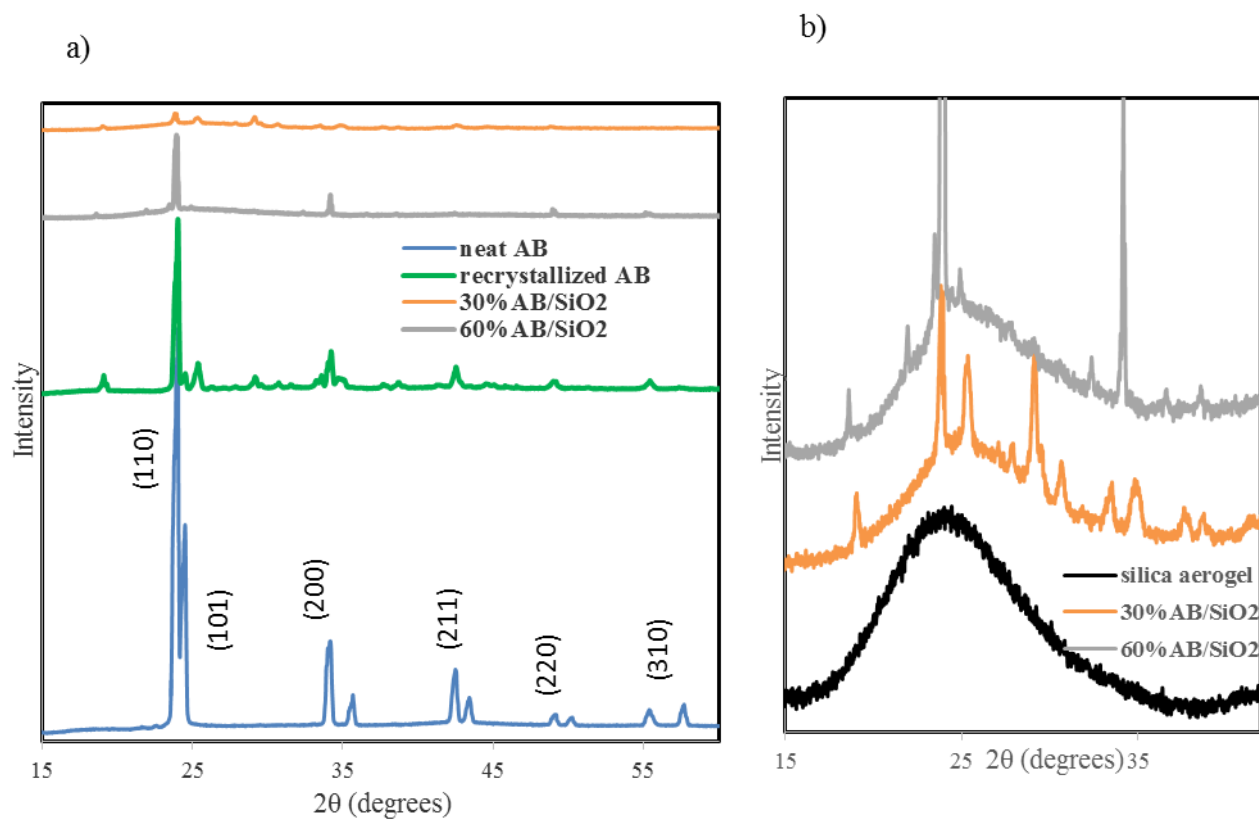
Figure 6. –a) XRD of neat ammonia borane, recrystallized ammonia borane and AB loaded in silica aerogel with different concentrations b) Amplification of XRD signal showing the characteristic pattern of silica aerogel. Curves are vertically displaced for clarity

735
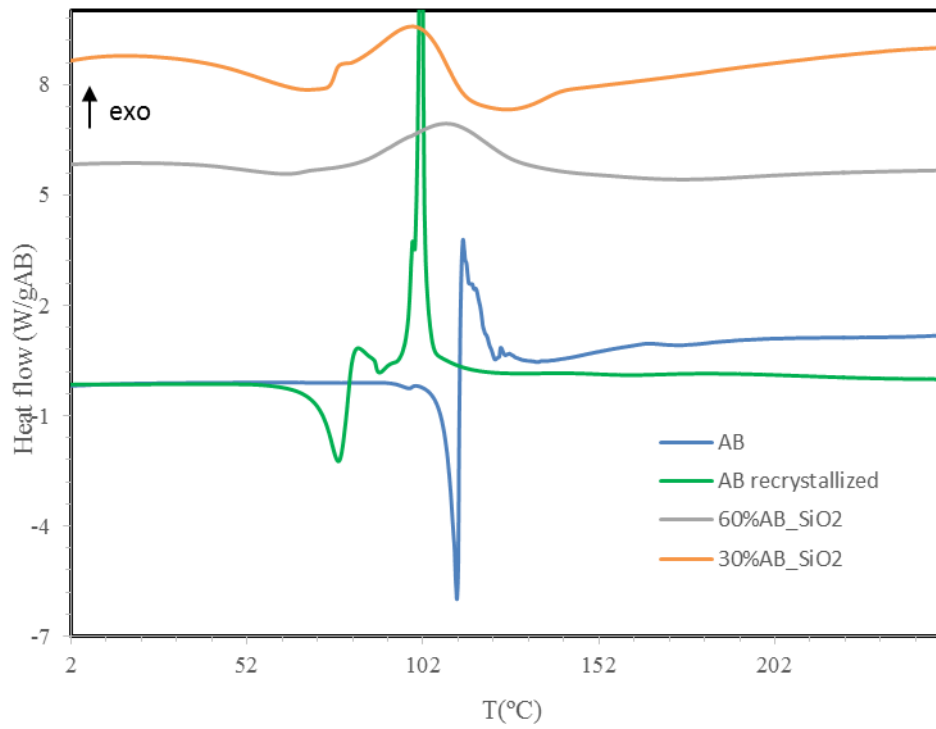
Figure 7. - DSC curves of AB and AB loaded in silica aerogel with different

concentration. The curves are normalized according to the weight of AB, and vertically
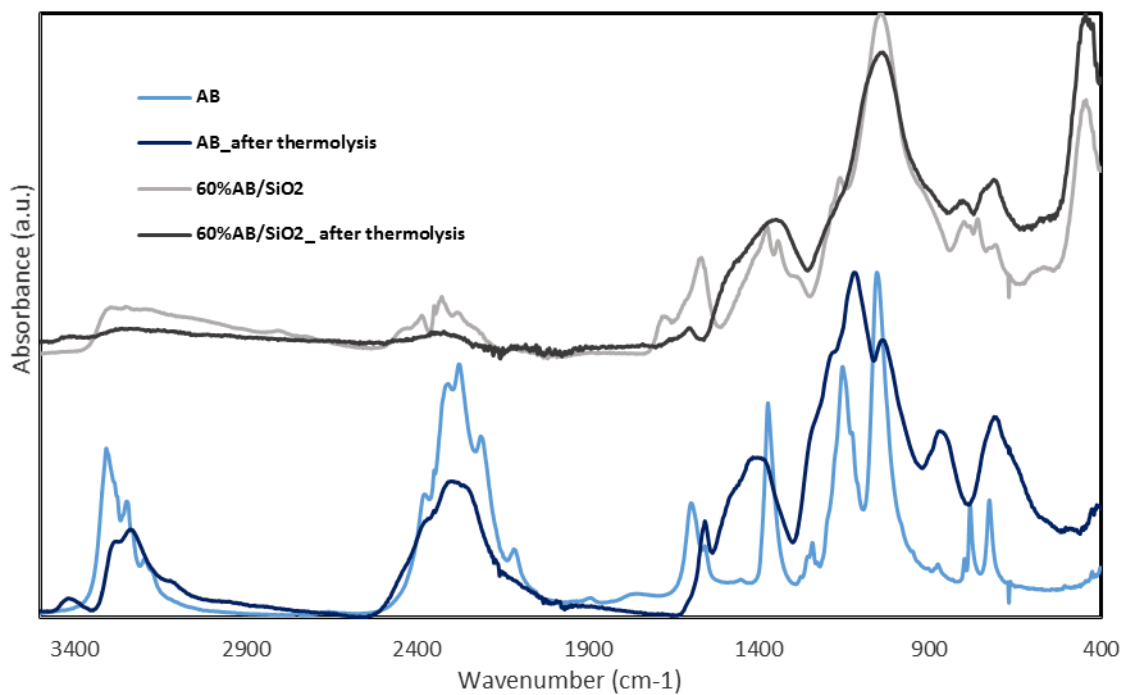
displaced for clarity.

739

740
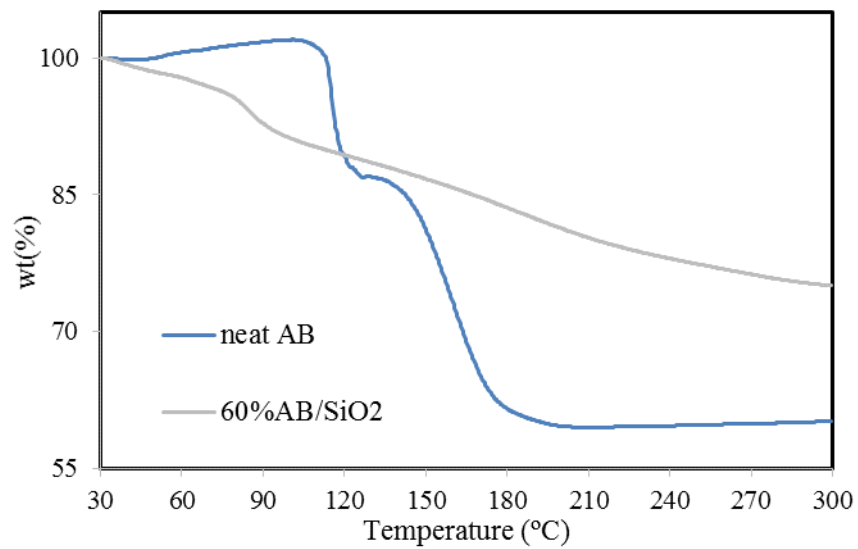
Figure 8. - TGA curves of AB and AB loaded in silica aerogel
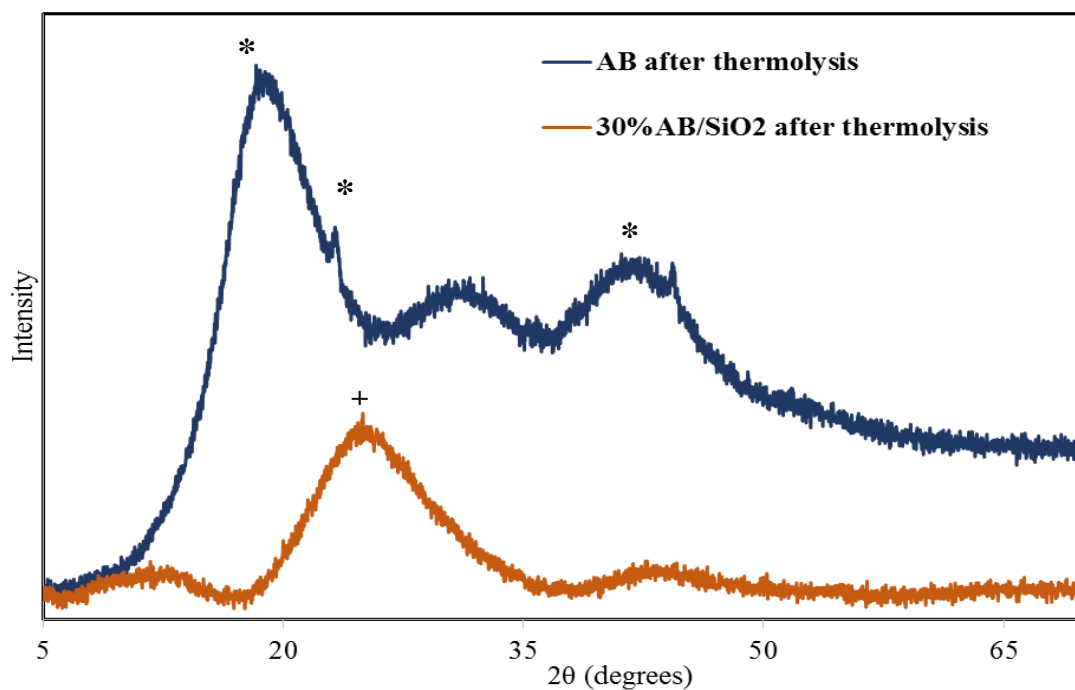
741

742

743
744   **Figure 9**. - FTIR spectra of neat AB and AB loaded in silica aerogel before and after

745   thermolysis dehydrogenation at 80ºC. Curves are vertically displaced for clarity

746

747

Figure 10. - XRD of neat AB and AB loaded in silica aerogel after thermolysis

dehydrogenation at 80ºC. * indicates the peaks related to polyaminoborane (PAB) and +
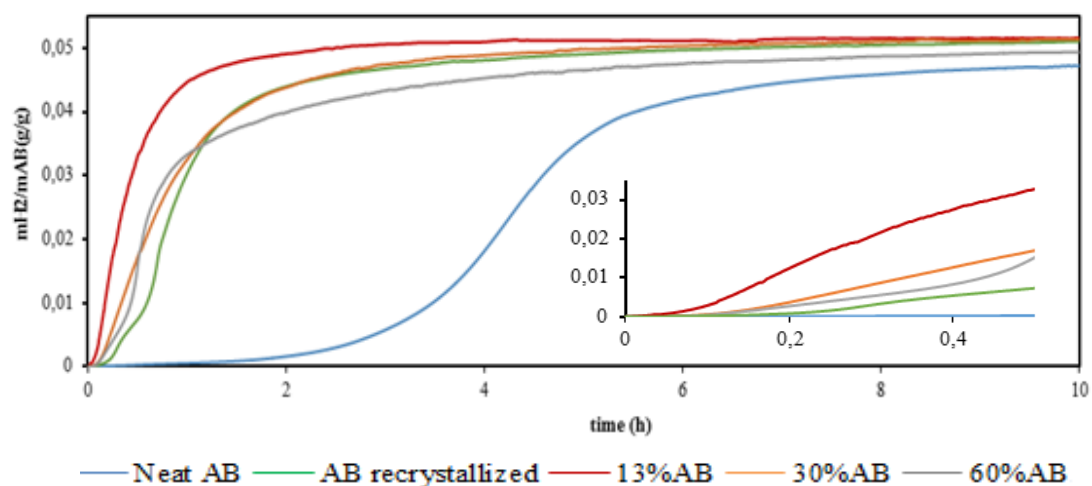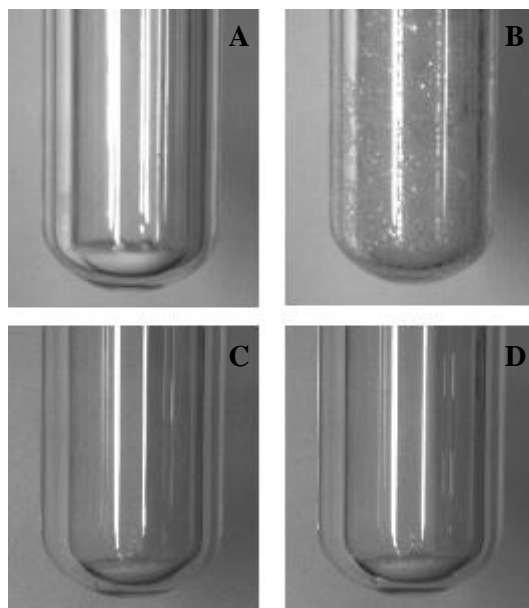
refers to amorphous silica peak

752

Figure 11. - Isothermal kinetic of hydrogen releases from AB and AB loaded in silica

753

aerogel with different concentrations at 80ºC. (The curves are normalized according to
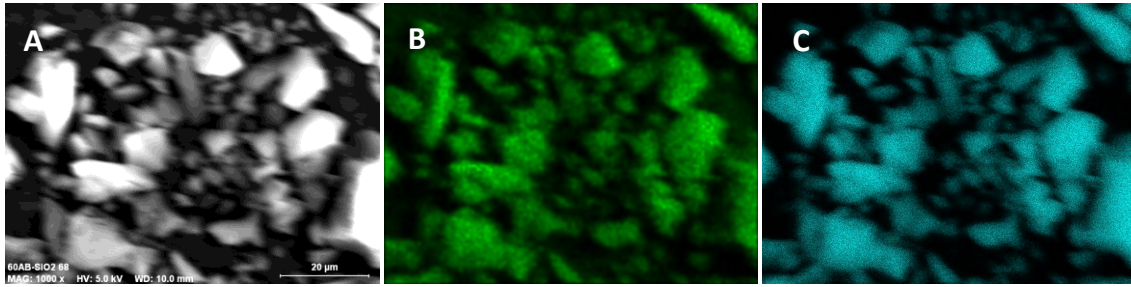
754

the amount of AB in the sample)

755

756

757

758

759   **Figure 12.-** Photographs of neat AB and 60%AB/SiO$_2$ before and after the

760   isothermal H$_2$ release by thermolysis at 80ºC a) neat AB before thermolysis, b)

761   neat AB after thermolysis, c) AB/SiO$_2$ before thermolysis, d) AB-SiO$_2$ after

762   thermolysis. Video clips of the thermolysis process are provided as

763   Supplementary Information

764

765

Figure 13.- SEM image of 60%AB/SiO$_2$ sample after thermolysis (A), with results of N

767 (B) and Si (C) mapping.